Electronic Supplementary Information

Rapid and Label-Free Bacteria Detection using Hybrid Tri-layer Dielectrics Integrated n-Type Organic Field Effect Transistor

Anamika Dey,[a] Ashish Singh,[a] Deepanjalee Dutta,[a] Siddhartha Sankar Ghosh[a,b,*] and Parameswar Krishnan Iyer [a,c,*]

[a]Centre for Nanotechnology,[b]Department of Biosciences & Biotechnology, [c]Department of Chemistry, Indian Institute of Technology Guwahati, Guwahati-781039, Assam, India.

Corresponding Author

*Prof. Parameswar Krishnan Iyer
[c]Department of Chemistry, Indian Institute of Technology Guwahati, Guwahati-781039, Assam, India. Fax: (+) 91 361 2582314. E-mail: pki@iitg.ac.in

*Prof. Siddhartha Sankar Ghosh
[b]Department of Biosciences & Biotechnology, Indian Institute of Technology Guwahati, Guwahati-781039, Assam, India. E-mail: sghosh@iitg.ac.in

Table of Contents

Experimental Procedures

1. Device fabrication method:

At the beginning of OFET device fabrication, microscope glass substrates were cut into 1 cm × 2.5 cm dimensions and then cleaned by dipping in acidic piranha solution (1:3 ratio of H_2O_2:H_2SO_4) for 1 hour. Further, the substrates were vigorously washed by de-ionized water for 8-10 times to remove the acidic layer and dried at 100°C on hot plate. Followed this, >200 nm Al-gate was thermally deposited through shadow mask. Nearly 13 nm of the upper surface of these thermally deposited Al films were then electrochemically oxidized to grow the first barrier type inorganic Al_2O_3 dielectric layer following previously reported cost effective anodic oxidation method.[1-3] The function of this barrier type Al_2O_3 dielectric layer is to reduce the gate leakage up to 5 μA and to prevent the direct contact of the second inorganic high-k TiO_2 dielectric layer to the gate electrode. For the second inorganic dielectric layer, colloidal solution of high-k TiO_2 was synthesized one night before to the device fabrication by using simple sol-gel method. The detail synthetic protocol of TiO_2 sol gel and its observed various thin film characteristics are given below (Figure S1). The solution was then spun on Al_2O_3 coated glass substrate and annealed at 110°C on a hot plate. It was observed that the synthesized TiO_2 was crystalline in nature and their thin films were very rough (σ_{rms}~4.11 nm) with visible cracks observed under various microscopic analyses (Figure S1d and Figure S2b). To reduce it, a very thin PMMA polymer dielectric layer, (the third dielectric layer), were coated [3% (w/v) from anisole, 3000 r.p.m.] on the top of these TiO_2 layers. Due to PMMA dielectrics, the roughness of the top surface of TiO_2 layers reduced very significantly (σ_{rms} ~1.39 nm) which were confirmed in layer-by-layer AFM analysis (Figure S2). This PMMA layer also helps to prevent the degradation of n-type semiconductor by protecting it from direct contact with the second dielectric layer. After the dielectric layer deposition, a 70 nm (±10 nm) PDI-C8 was thermally deposited. Finally, followed by ~80 nm source-drain silver contacts deposition at room temperature (RT) above the PDI-C8 through the shadow mask in order to calculate the three terminal properties of the devices.

2. TiO_2 sol-gel dielectric synthetic protocol:

Colloidal high-k TiO_2 dielectric is synthesized by using simple Sol-Gel method. A solution of Titanium (IV) Isopropoxide in Isopropanol was added to a solution of water and glacial acetic acid which was placed in an ice bath prior to the addition for about 30 min. After the addition the mixture was constantly stirred and a cloudy white precipitate was observed. The precipitate was then placed in a water bath at 80°C with constant stirring to obtain a gel like entity which became milky on cooling down. This colloidal solution obtained was placed in a sealed glass flask and kept in a vacuum oven at 200°C for 12 hours and then cooled to the room temperature to obtain white colloidal TiO_2 solution. The solution obtained was stable for a month and could be used after stirring. The end product was a white solution of TiO_2 with a bluish ting.

Results and Discussion

3. Thin film growth structure of TiO_2 dielectric:

The synthesized TiO_2 sol-gel nanoparticle was characterized by various experimental techniques which are shown in Figure S1. The crystalline nature of TiO_2 thin film was confirmed by using high power (18 kW) X-ray diffractometer. Figure S1a displays both the

UV-vis absorption spectra (λmax =306.13 nm) and X-ray diffraction (XRD) patterns of TiO_2 thin film. It is evident that the sharp diffraction peaks observed in the regions from 2θ= 20° to 80° support the formation of small size, polycrystalline, pure anatase phase of the TiO_2 (JCPDS card no. 21-1272) nanoparticle. The crystalline size (D) of TiO_2 NPs was calculated by using the well-known Debye-Scherer formula, for respective different diffraction peak positions. The highest particle size at 2θ= 25° is calculated as ~16.4 nm which also has good agreement with the size observed in case of TEM analysis (~15 nm, shown in Figure S1b). To further study the crystalline nature, we investigated the High-Resolution Transmission Electron Microscope (HRTEM) images and Selected Area Electron Diffraction (SAED) patterns of TiO_2 sol gel which are shown in Figure S1c. Closer observation of the HRTEM image reveals that, the interplanar spacing is about 0.35 nm, which is exactly matching with the value calculated from the XRD peak at 2θ = 25°. The polycrystalline nature of TiO_2 is also confirmed by SAED patterns as shown in the inset of Figure S1c. Figure S1d represent the FESEM image of TiO_2 thin film deposited on anodized Al_2O_3 layer. As the film is very rough in nature and visible cracks are observed, this analysis revels that without any additional buffer layer modification, bare TiO_2 thin film is not suitable for smoother active layer thin film deposition.

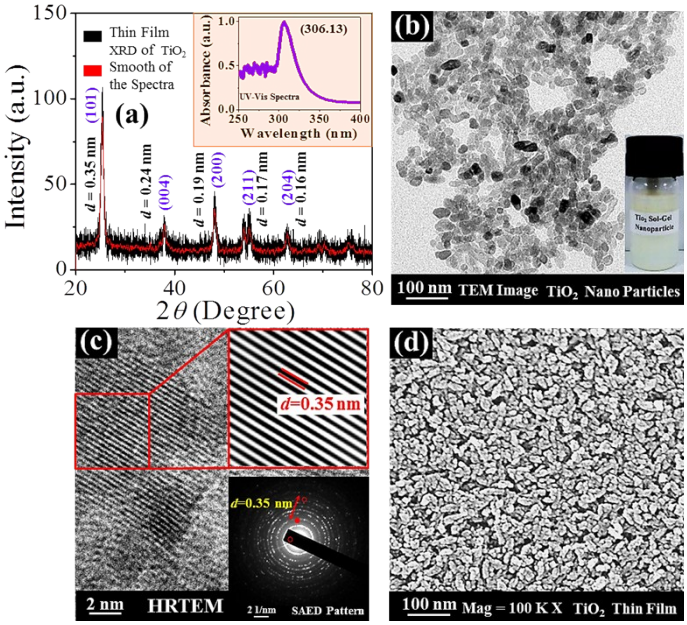

Figure S1 (a) Thin film XRD spectra of TiO_2 sol-gel. Inset: thin film UV-Vis absorption spectra. (b) TEM image of TiO_2. Inset: Synthesizes TiO_2 sol-gel. (c) HRTEM spectra of TiO_2 sol gel. Inset: SAED pattern. Showing *d*-spacing, *d*= 0.35 nm. (d) FESEM image of TiO_2 over anodized Al_2O_3 dielectric layer.

4. AFM analysis:

The layer-by layer AFM images of the PDI-C8 based OFET are shown in Figure S2. It has been observed that the r.m.s. surface roughness of bare Al_2O_3 (~3.04 nm, Figure S2a) and Al_2O_3/TiO_2 (~4.11 nm, Figure S2b) are quite high but after PMMA coating it reduces to ~1.39 nm (Figure S2c). Further, after the deposition of PDI-C8 it again slightly increases to ~2.34 nm due to the uneven film formation of PDI-C8 (Figure S2d).

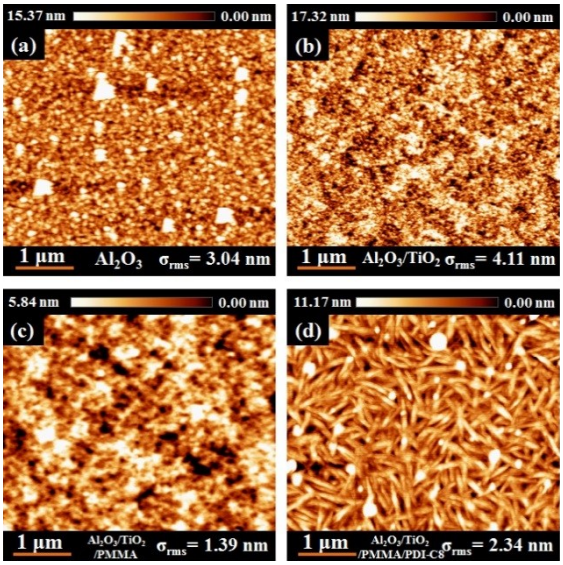

Figure S2 Layer-by-layer AFM imagers of (a) anodized Al_2O_3 (b) Al_2O_3/TiO_2 sol gel (c) Al_2O_3/TiO_2 sol gel/PMMA and (d) Al_2O_3/TiO_2 sol gel/PMMA/ PDI-C8 at 90°C substrate temperature deposited on glass substrate.

5. Device standardization and characterization:

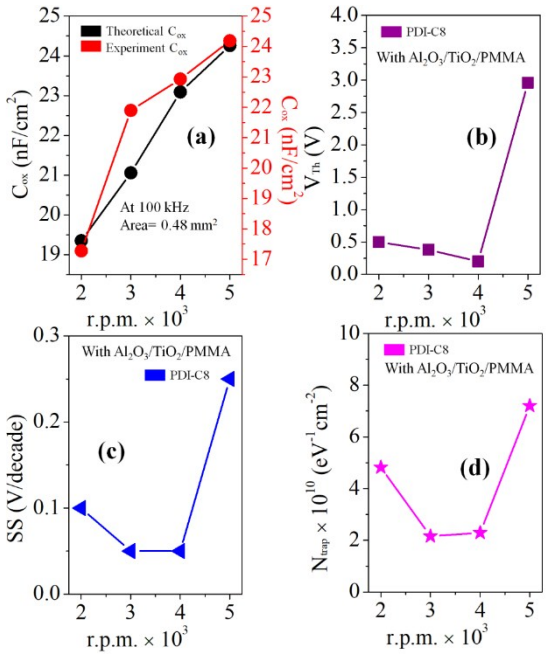

Figure S3 Graphical presentation of (a) capacitance density at 100 kHz and variation of (b) V_{Th} (c) SS and (d) charge trap density with respect to TiO_2 spin coating speed (r.p.m) of PDI-C8 based Al_2O_3/TiO_2/PMMA contained organic field effect transistors.

The structure of the n-type OFET was standardized step-by-step prior to the bacteria detection by varying the thickness of TiO_2 with different r.p.m. 2000, 3000, 4000 and 5000 respectively with constant thickness of $A_{l2}O_3$ and PMMA. It was observed that the overall capacitance density (C_{ox}) of the tri-layer dielectric layer increases systematically with increasing the r.p.m value (Figure S3a). Though the V_{Th} values are also showing systematic

decrement with the decrease in TiO_2 thickness (Figure S3b), at 5000 r.p.m. it's again increased.

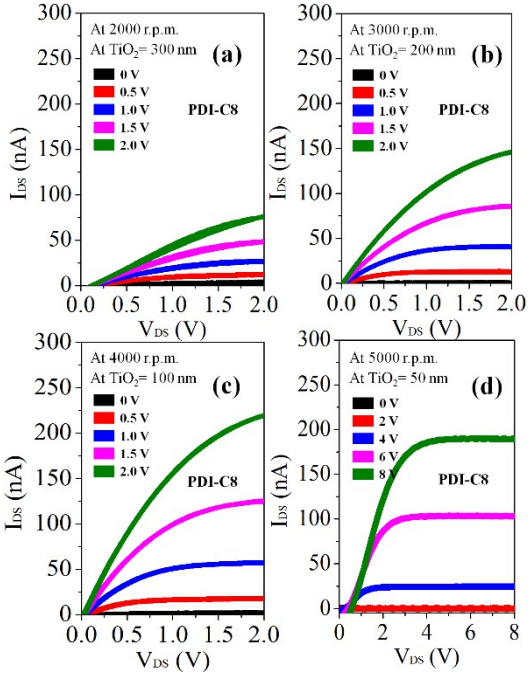

Figure S4 Drain Characteristics of PDI-C8 with respect to different TiO_2 spin coating speed (r.p.m) (a) 2000 r.p.m. (b) 3000 r.p.m. (c) 4000 r.p.m. and (d) 5000 r.p.m. respectively.

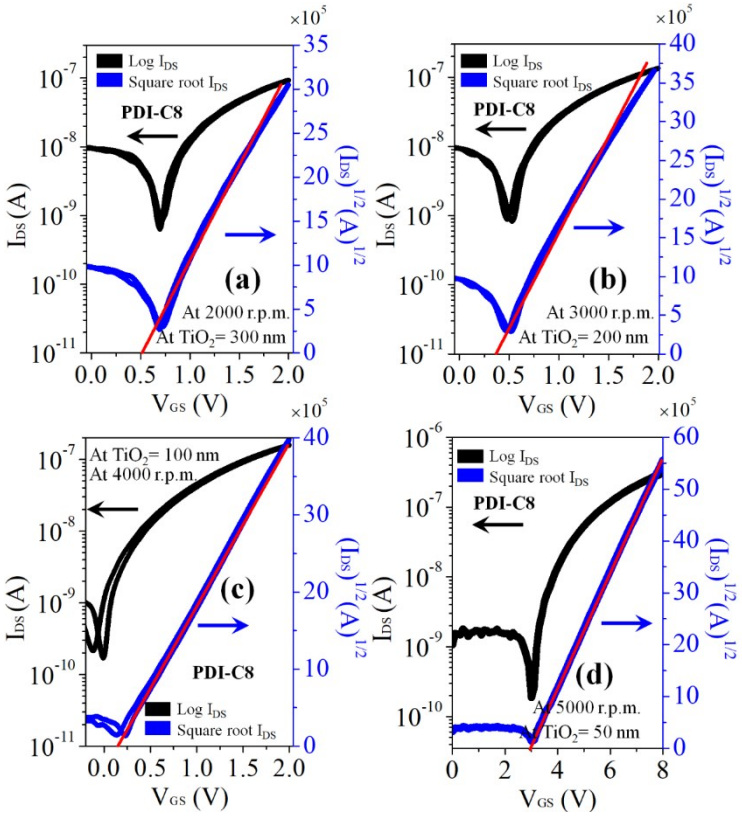

Figure S5 Transfer Characteristics of PDI-C8 with respect to different TiO_2 deposition speed (r.p.m) (a) 2000 r.p.m. (b) 3000 r.p.m. (c) 4000 r.p.m. and (d) 5000 r.p.m. respectively.

Similar anomalous behavior also observed in the drain and transfer characteristics (Figure S4 and Figure S5). From Figure S4, it was observed that the drain current increases up to 3000 r.p.m. and reached maximum at 4000 r.p.m and then started to decrease at 5000 rpm. This is because, at 2000 and 3000 r.p.m., due to the high thickness of the second dielectric layer, less numbers of charges are able to accumulate at the channel. At 4000 r.p.m. the thickness of TiO_2 and PMMA becomes almost equal (~ 100 nm) and since TiO_2 is a high-k dielectric material compare to PMMA, the dominancy of TiO_2 become more in this case. As a result, I_{DS} increase. Further decreasing the thickness of TiO_2 (~50 nm at 5000 r.p.m.), the dominancy of PMMA becomes more since all the dielectrics are connect with each other with a series combination. As a result, due to very less influence of TiO_2, the OFETs in this case is exhibiting higher operating voltages and V_{Th} values, which is further, decreases the charge carrier mobility. These results are also supported by Figure S3c and Figure S3d. As the influence of TiO_2 decreases the trap density increases in case of 5000 r.p.m. The detail OFETS performances of the fabricated devices on all different r.p.m. of TiO_2 are summarized in Table S1.

Table S1. Summary of the device performance of hybrid tri-layer dielectrics contained PDI-C8 based ultra-low operating voltage n-type OFET.

Substrate	r.p.m.	C_{ox} (nF/cm^2)	V_{Th} (V)	μ (cm^2/V s)	I_{ON}/I_{OFF} Ratio	$N_{trap} \times 10^{10}$ (eV^{-1} cm^{-2})	SS (V/ decade)
Glass	2000	17.28	0.50	0.20	10^3	4.8	0.1
	3000	21.90	0.38	0.25	10^3	2.3	0.05
	4000	22.93	0.20	0.30	10^4	2.2	0.05
	5000	24.19	2.96	0.03	10^3	7.2	0.25
PET	4000	21.09	0.15	0.27	10^3	2.0	0.05

6. Electrical stability and compatibility study:

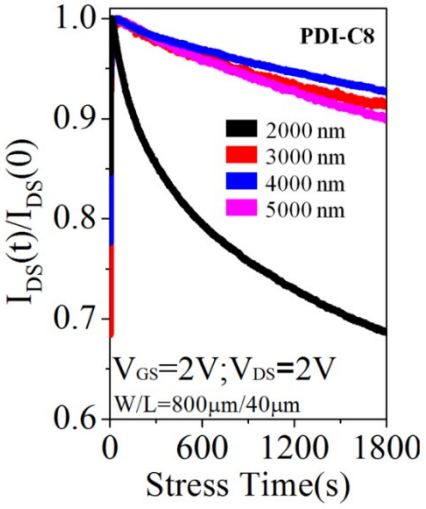

Figure S6 Graphical representations of the time dependence of the normalized drain current $I_{DS}(t)/I_{DS}(0)$ of PDI-C8 gated with Al_2O_3/TiO_2/PMMA tri-layer dielectrics system with respect to different TiO_2 deposition speed (r.p.m) (a) 2000 r.p.m. (b) 3000 r.p.m. (c) 4000 r.p.m. and (d) 5000 r.p.m. respectively.

In order to check the electrical stability of the PDI-C8 based OFETs under tri-layer dielectric system, the time-dependent decay of I_{DS} under a DC bias stress with V_{DS}= V_{GS}= 2 over 1200 sec (Figure S6) are recorded. It was observed that the decay of drain current, I_{DS} at 2000, 3000 and 4000 r.p.m. are

very less (~5-10%). But at 5000 r.p.m. decay of I_{DS} is more (~30%). This is because of higher trapping of charges at the dielectric-semiconductor interface. Further, in order to check the compatibility of this dielectric material in flexible substrate we fabricate the same devices on PET substrate followed by the procedure mentioned the device fabrication method. It has been observed that this device configuration is also compatible with flexible substrate showing the same performance as observed in case of glass substrate (Figure S7). From the overall performances of the device it can be strongly concluded that this device this dielectrics architecture is one of the best and stable device configurations for ultra-low operating voltage, n-type organic field effect transistor.

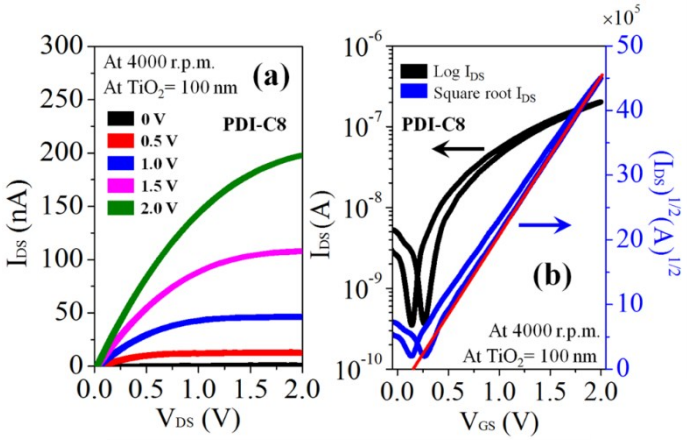

Figure S7 OFET characteristic curves of PDI-C8 with gated with Al_2O_3/TiO_2/PMMA tri-layer dielectrics system on flexible PET substrate.

7. FESEM images:

For the confirmation of the presence of bacteria on the channel, FESEM image was taken after the adsorption which are shown below in Figure S8-

.

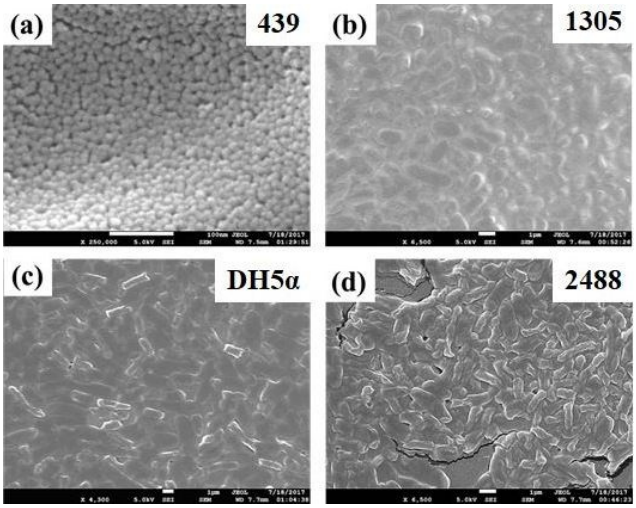

Figure S8 FESEM images of the bacteria layers (with 10^{-3} dilution) on 40 μm channel of n-type OFETs.

8. OFET device architecture:

The n-type OFET based bacteria sensor were fabricated on bottom gate top contact configuration, which are shown below in Figure S9.

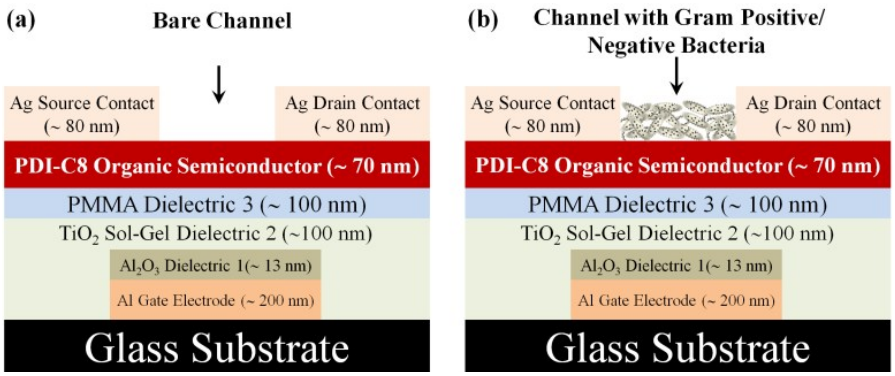

Figure S9 Schematic representation of the ultra-low operated n-type OFETs (a) Bare Device and (b) Device with bacteria at the channel.

9. Bacterial plating:

After OFET based sensing device characterization the number of colonies in minimum dilution was examined which are shown below in Figure S10.

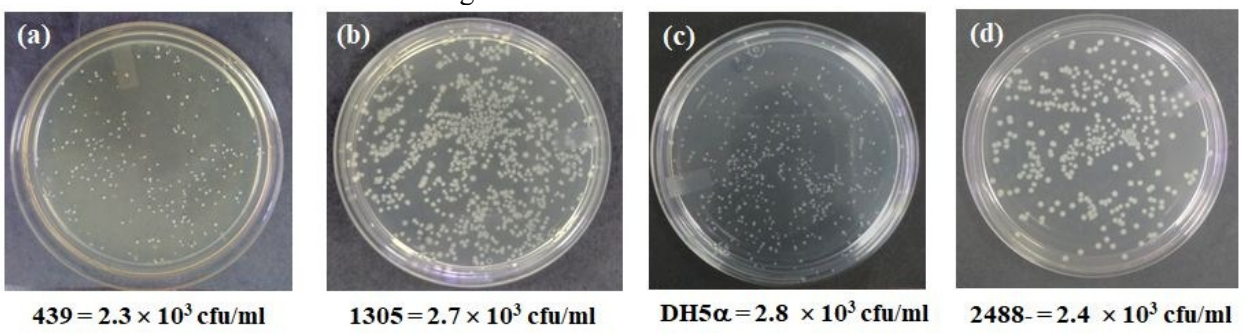

Figure S10 Plating images of (a) 439, (b) 1305, (c) DH5α and (d) 2488 bacteria.

10. Table S2. Summary of recent literature data on OFETs based Bacteria Sensor.

Method	Target analyte(s)	Transducer Signal	Sensor assembly	Bioreceptor (s)	LOD	Analyte(s)	Ref.
Optical Biosensor	Salmonella enterica, Listeria monocytogenes, Escherichia coli O157:H7	Fluorescence	Antibodies linked via biotin/avidin to optical fibers	Polyclonal antibody for capture, fluorescent monoclonal antibody or aptamer against surface protein InlA as reporter	10^3 cfu/ml	Artificially contaminated meat samples	27, 28
	Escherichia coli	Surface plasmon resonance	Bacteriophage covalently bound to SiO_2 optical fibers	T4 bacteriophage	10^3 cfu/ml	Bacteria in buffer	29
	Shewanella oneidensis	Surface-enhanced Raman scattering	Silver nanoparticles sandwiched by analyte binding on optical fiber tip	NA	10^6 cells/ml	Bacteria in buffer	30
Mechanical biosensors	E. coli O157:H7	Quartz crystal microbalance	Antibody for capture and antibodyfunctionalized nanoparticles	Anti-E. coli antibody	10^6 cells/ml	Bacteria in buffer	31

			for signal enhancement				
	Bacillus anthracis	Quartz crystal microbalance	Protein A/antibody-functionalized SAM on gold	Anti-B. anthracis antibody	1×10^3 cfu or spores/ml	Vegetative cells and spores	32
	Vibrio cholerae O1 Microcantilever	Microcantilever/ Dynamic Force Microscopy	Antibody-functionalized SAM on gold	Anti-V. cholera antibody (monoclonal)	1×10^3 cfu/ml	Bacteria in buffer	33
Method	Bacterium	Transducer	Technique	Bioreceptor	LOD	Comments	Ref.
Potentiometric Biosensor	Sulfate-reducing bacteria	Glassy carbon electrode	Potentiometric stripping analysis	None	2.3×10 to 2.3×10^7 cfu/ml	Need bacterial processing	34
	Staphylococcus aureus	Single-walled carbon nanotubes	electron motive force	Aptamer	8×10^2 cfu/ml	Bacterium-spiked pig skin	35
Amperometric Biosensor	E. coli	Photolithographic gold	Immunomagnetic/amperometric in flow cells	Antibody	55 cells/ml in PBS, 100 cells/ml in milk	No contact of biocomponent with sensor	36
	Heat-killed E. coli	Saturated calomel electrode	Amperometric detection of secondary antibody with glucose oxidase	Biotinyl antibody	3×10^1 to 3.2×10^6 cfu/ml, down to 15 cfu/ml	Labeling needed but tested in synthetic stool	37
Method	Bacterium	Transducer	Chemistry	Bioreceptor	LOD	Comments	Ref.
Impedimetric electrochemical biosensors	E. coli	7% gold-tungsten plate wire	Polyethyleneamine-streptavidin	Biotinyl antibody	10^3–10^8 cfu/ml	Dielectrophoretic force and antibody–antigen interaction was developed for detection and quantification of foodborne pathogenic bacteria	38
	E. coli	Screen-printed carbon microarrays	1-ethyl-3-(3-dimethylaminopropyl) carbodiimide (EDC)	Bacteriophage	10^4 cfu/ml for 50µl samples	Acidic media of EDC by applying a potential of +2.2 V to the working electrode	39
	Sulfate-reducing bacteria	ITO	Chitosan-reduced grapheme sheet	Bioimprint of bacteria	1.0×10^4 to 1.0×10^8 cfu/ml	RGSs-CS hybrid film served as a platform for bacterial attachment	40
Organic field effect transistor on glass or flexible substrates	Detection of gram positive and negative bacteria. Distinguishing them	OFET device. (a) Change in mobility (b) Change in threshold voltage (c) Change in operating voltage	Mechanistic investigation on the role of cell walls of bacteria.	No antibody requirement, no imprinting required. Direct addition of live bacteria solution.	10^3 cfu/ml	No labeling, no bioreceptor antibody	**Present work**

References

1. Dey A, et al. (2016) High performance, low operating voltage n-type organic field effect transistor based on inorganic-organic bilayer dielectric system. *J. Phys.: Conf. Ser.* 704:1-8.
2. Dey A, et al. (2016) Photosensitive organic field effect transistors: the influence of ZnPc morphology and bilayer dielectrics for achieving a low operating voltage and low bias stress effect. *Phys. Chem. Chem. Phys.* 18: 32602-32609.
3. Dey A, et al. (2017) High-performance ZnPc thin film-based photosensitive organic field-effect transistors: influence of multilayer dielectric systems and thin film growth structure. *ACS Omega* 2:1241-1248.